

Article

Adsorption of Pb^{2+} and Cd^{2+} in Agricultural Water by Potassium Permanganate and Nitric Acid-Modified Coconut Shell Biochar

Hengji Qin ¹, Xiaohou Shao ^{1,*}, Hiba Shaghaleh ² , Wei Gao ³ and Yousef Alhaj Hamoud ⁴ 

¹ College of Agricultural Science and Engineering, Hohai University, Nanjing 211100, China; qinhengji@hhu.edu.cn

² College of Environment, Hohai University, Nanjing 210098, China; hiba-shaghaleh@njfu.edu.cn

³ North Information Control Group Co., Ltd., Beijing 100044, China

⁴ College of Hydrology and Water Resources, Hohai University, Nanjing 210098, China; yousef-hamoud11@hhu.edu.cn

* Correspondence: shaoxiaohou@163.com

Abstract: Biochar prepared from agricultural waste resource coconut shells was used as the original charcoal, which was oxidatively modified and characterized using batch adsorption tests before and after modification by SEM, FTIR, surface area, and elemental analyses. The removal capacity and adsorption mechanism of the modified biochar for Pb^{2+} and Cd^{2+} in water were investigated, and its adsorption kinetics and thermodynamics were discussed. The findings demonstrated that the specific surface area of potassium permanganate and nitric acid-modified coconut shell carbon (MHBC) is 3.02 times than that of the coconut shell carbon (BC). The kinetic data of adsorption of Pb^{2+} and Cd^{2+} on MHBC were more in accordance with the pseudo-second order kinetic model, indicating that chemical adsorption played a dominant role, and the adsorption rate gradually tended to balance with a decrease in solution ion concentration. The isothermal thermodynamic data of the adsorption of Pb^{2+} and Cd^{2+} by MHBC conformed to the Langmuir model. At pH = 5.5, the maximum adsorption capacities of Pb^{2+} and Cd^{2+} were 160.41 $mg \cdot g^{-1}$ and 47.46 $mg \cdot g^{-1}$, respectively. Thermodynamic parameter fitting showed that the process of adsorption of Pb^{2+} and Cd^{2+} by MHBC is a spontaneous endothermic reaction. The higher the temperature is, the stronger the adsorption capacity is. When the ions coexist, Pb^{2+} and Cd^{2+} have obvious competitive adsorption, and Pb^{2+} has a significant competitive advantage. Among them, MHBC has high adsorption and good reusability for Pb^{2+} and Cd^{2+} , and has good practical application prospects.

Keywords: adsorption; lead; cadmium; modification; biochar; water environment



Citation: Qin, H.; Shao, X.; Shaghaleh, H.; Gao, W.; Hamoud, Y.A. Adsorption of Pb^{2+} and Cd^{2+} in Agricultural Water by Potassium Permanganate and Nitric Acid-Modified Coconut Shell Biochar. *Agronomy* **2023**, *13*, 1813. <https://doi.org/10.3390/agronomy13071813>

Academic Editors: Ting Li, Ming Li and Kang Tian

Received: 12 June 2023

Revised: 30 June 2023

Accepted: 5 July 2023

Published: 7 July 2023



Copyright: © 2023 by the authors. Licensee MDPI, Basel, Switzerland. This article is an open access article distributed under the terms and conditions of the Creative Commons Attribution (CC BY) license (<https://creativecommons.org/licenses/by/4.0/>).

1. Introduction

With the rapid development of the industrial and agricultural economy and the intensified pace of urbanization, environmental heavy metal pollution has become one of the major environmental issues in China; in particular, the pollution situation involving lead (Pb) and cadmium (Cd) has become increasingly severe [1,2]. Pb, Cd, and their compounds enter into the food chain through bioconcentration and biomagnification, which endanger the survival of plants and animals and the ecological environment, and consequently have a negative impact on human health and life activities [3,4]. At the same time, these processes cause serious economic losses. According to incomplete statistics, the direct economic loss caused by heavy metal pollution in water bodies in China has exceeded CNY 20 billion every year since 2014 [5–8]. Therefore, the control of Pb and Cd pollution in the aquatic environment has attracted increasing attention [9]. Adsorption and precipitation are the most common methods to remove heavy metals from the water environment, which have the characteristics of low cost, simple operation, and renewability [10–13]. At present, the

development of adsorption materials with high adsorption capacities for Pb and Cd is one of the key issues in the field of remediation of heavy metal pollution in water.

Biochar is a kind of porous carbon-rich material made by the pyrolysis of biomass under oxygen-limiting conditions [14]. Numerous studies have revealed that biochar is a good adsorption material, and can effectively adsorb heavy metals in the environment [15–18]. Doumer [19] studied biochar prepared with bagasse and coconut shells as raw materials, which can remove up to 95% of Cd^{2+} and Pb^{2+} in water. The adsorption of heavy metals by biochar is related to their physicochemical properties; it has a large specific surface area, rich pore structure, diverse surface functional groups, and a large ion exchange capacity [20,21]. The specific surface area and pore structure of biochar are driven by pyrolysis conditions such as pyrolysis temperature and residence time [18,22,23]. However, in the production process, it is easy to mix with impurities to produce coating, which affect the original structure and physical and chemical properties, thus reducing its ability to adsorb heavy metals. Some studies have shown that chemical modification can optimize the physicochemical properties and enhance the adsorption capacity of biochar. Peng et al. [24] studied the adsorption of phosphoric acid-modified pine sawdust biochar on Cd^{2+} and Cu^{2+} in water. After modification, the number of oxygen-containing functional groups and the specific surface area were increased, and the affinity for heavy metal ions was improved. Nicola et al. [25] made a magnetic composite material wrapped with silica. The maximum adsorption capacity of this material to Pb^{2+} in aqueous solution reached $14.9 \text{ mg}\cdot\text{g}^{-1}$, and had a low cost advantage. Wongrod et al. [26] studied the adsorption of Pb^{2+} in water by KOH-modified biochar, which increased the specific surface area, cation exchange capacity, and pH value of biological carbon at the zero charge point, and the adsorption capacity increased by 45.21% after modification. Ianasi et al. [27] synthesized a magnetic nanocomposite material for the removal of Cd^{2+} in aqueous solution. The highest specific surface area of the material reached $680 \text{ m}^2\cdot\text{g}^{-1}$, and the main adsorption was monolayer adsorption. Li et al. [28] investigated the adsorption mechanism of KMnO_4 -modified biochar on U(VI), and the increase in oxygen-containing functional groups improved the renewability of the biochar. Salam et al. [29] studied the desorption of Cd^{2+} in aqueous solution by new nano-sized zero-valent iron nanoparticles. In addition to the first-order and second-order chemical kinetics, there are two paths or two reactions in the adsorption process. El-Banna et al. [30] studied the removal effect of nitric acid and potassium permanganate-modified biochar on the toxicity of Pb^{2+} -stressed aquatic plants, and the affinity of the modified biochar for Pb^{2+} was significantly increased.

The coconut shell is a rich resource from tropical agricultural waste [31,32], and its unreasonable utilization easily leads to resource waste and environmental pollution. However, when it is used in biochar preparation for resource utilization, it offers a wide range of raw materials, a moderate price, reproducibility, and good environmental performance. The adsorption impact of coconut shell carbon on heavy metal ions is substantial. The adsorption effect of coconut shell carbon on Li^+ in water increased by $39.28 \text{ mg}\cdot\text{g}^{-1}$ through MnO_2 modification [33], and the removal rate of Cd^{2+} in soil by coconut shell carbon treated by pickling and ultrasound increased by 30.1% [34]. The modification of biochar with ammonia and nitric acid increased the adsorption capacity of Pb^{2+} by 113.1% [35]. Therefore, the preparation of biochar from coconut husks as a raw material for the treatment of heavy metals in polluted water has good effects, which are of great practical significance while reducing environmental pollution.

In summary, in order to improve the utilization of agricultural waste resources, it is necessary to optimize the adsorption performance of coconut shell carbon for Pb^{2+} and Cd^{2+} in water, simplify the operation steps, and speed up the adsorption process. This study used potassium permanganate and nitric acid to prepare MHBC, investigated the removal performance of MHBC for Pb^{2+} and Cd^{2+} in a water environment, and analyzed the adsorption capacity of MHBC for Pb^{2+} and Cd^{2+} in an agricultural water environment via characterization. The effects of the amount of MHBC, temperature, initial pH, and

competing ions on the removal efficiency of Pb^{2+} and Cd^{2+} were studied. The repeated utilization of MHBC was evaluated using adsorption resolution.

2. Materials and Methods

2.1. Test Materials

The coconut shells (purchased from Hainan coconut products factory) were washed with deionized water, dried in an oven (DHG-89F, CN) at 105 °C to a constant weight, ground, placed into a crucible, and then carbonized (QXL-201, CN) at 500 °C (heating rate of 10 °C·min⁻¹) in a muffle furnace for 2 h. Nitrogen was introduced as a protective gas during the process. Then, the product was cooled to room temperature, removed, and ground through a 100-mesh screen to obtain BC, which was dried and stored for future use.

An amount of 10 g of coconut shell carbon was weighed, impregnated into 1000 mL of a certain concentration of a potassium permanganate and nitric acid mixture solution, then placed on a constant temperature shaking table (TS-211b, CN) that shook at 25 °C for 24 h. The product after impregnation was repeatedly cleaned with ultra-pure water to neutral, and then placed in an oven to dry at 105 °C to a constant weight to become the modified coconut shell carbon (MHBC) and stored for future use.

An appropriate amount of $Pb(NO_3)_2$ and $Cd(NO_3)_2$ were dissolved in 1000 mL of pure water to prepare the 2000 mg·L⁻¹ Pb^{2+} and Cd^{2+} reserve solution; then, the reserve solution was diluted with deionized water to form the required Pb^{2+} and Cd^{2+} working solution.

In order to optimize the modification process of MHBC, different ratios of potassium permanganate and nitric acid were set. MH1, MH2, and MH3 mean that the ratios of $KMnO_4:HNO_3 = 0.3:1.0, 0.3:2.0, 0.3:3.0 \text{ mol}\cdot\text{L}^{-1}$, respectively. The removal rate of the Pb^{2+} and Cd^{2+} single-system solution was used as the reference index to determine the MHBC optimization conditions, using the single factor cross test.

2.2. Characterization of Biochar

An FEI Quanta200 scanning electron microscope (SEM) was used to show the morphological composition of the coconut shell charcoal before and after modification, and FTIR (Nicolet Nexus 470, Thermo electric Ltd., Waltham, MA, USA) was used to scan the coconut shell charcoal at 400–4000 cm⁻¹ to analyze the functional group changes of coconut shell charcoal before and after modification. The specific surface area and pore size of the coconut shell charcoal before and after modification were analyzed by a specific surface area analyzer; the main constituent elements of coconut shell charcoal before and after modification were determined by an element analyzer (Vario EL III, GER); the zeta potential value was measured with a zeta potential tester (SurPASS 3, AT); and the content of oxygen-containing functional groups on the surface was determined via Boehm titration.

2.3. Adsorption Experiment

The adsorption of Pb^{2+} and Cd^{2+} in solution by MHBC was studied using batch experiments, and the experiments were repeated 3 times in each group. Unless otherwise specified, the experiment mixed MHBC with the diluted Pb^{2+} and Cd^{2+} single-system solution at a solid–liquid ratio of 1.25 g·L⁻¹ at 25 °C and pH = 5.5 (The Pb^{2+} and Cd^{2+} single-system solution were diluted to 200 mg·L⁻¹, and then 40 mL mixed with 50 mg of MHBC, respectively), oscillated at 160 rpm on a constant temperature oscillating shaker for 12 h; then, the filtrate was collected using a membrane separation method. The residual Pb^{2+} and Cd^{2+} were determined with an inductively coupled plasma atomic emission spectrometer (ICP-OES, Agilent710, Agilent Technologies Ltd., Santa Clara, CA, USA). The adsorption amount and rates of MHBC for Pb^{2+} and Cd^{2+} are calculated by Equations (1) and (2), respectively:

$$q_e = \frac{(c_0 - c_e)v}{m} \quad (1)$$

$$\text{Adsorption}(\%) = \frac{c_0 - c_e}{c_0} \times 100\% \quad (2)$$

In the equation, q_e is the adsorption amount at equilibrium, in $\text{mg}\cdot\text{g}^{-1}$, c_0 and c_e are the initial and equilibrium concentrations of Pb^{2+} and Cd^{2+} , $\text{mg}\cdot\text{L}^{-1}$, v is the solution volume, L, and m is the amount of adsorbent added, g.

The adsorption kinetics tests were sampled in 5–720 min and analyzed using the pseudo-first-order model, the pseudo-second-order model, and the Weber–Morris model.

The pseudo-first-order model is represented as follows:

$$\ln(q_e - q_t) = \ln q_e - k_1 t \quad (3)$$

The pseudo-second-order model is as follows:

$$\frac{t}{q_t} = \frac{t}{q_e} + \frac{1}{k_2 \cdot q_e^2} \quad (4)$$

The Weber–Morris is represented as the following:

$$q_t = kt^{1/2} + C \quad (5)$$

In the equation, q_e is the equilibrium adsorption amount, in $\text{mg}\cdot\text{g}^{-1}$. q_t is the adsorption capacity at t time, in $\text{mg}\cdot\text{g}^{-1}$. k is the intra-particle diffusion rate constant, in $\text{mg}\cdot\text{g}^{-1}\cdot\text{h}^{-1/2}$. k_1 is the pseudo-first-order adsorption kinetic rate constant, in h^{-1} . k_2 is the pseudo-second-order adsorption kinetic rate constant, in $\text{g}\cdot\text{mg}^{-1}\cdot\text{h}^{-1}$. t is the adsorption time, h. C is a constant.

The concentration of Pb^{2+} and Cd^{2+} in the initial solution was adjusted to 25–200 $\text{mg}\cdot\text{L}^{-1}$ at 25 °C, 35 °C, 45 °C, and 55 °C, respectively. The isothermal adsorption was tested using the Langmuir and Freundlich models.

The Langmuir model is as follows:

$$\frac{c_e}{q_e} = \frac{1}{q_m} c_e + \frac{1}{q_m k_L} \quad (6)$$

The Freundlich model is as follows:

$$\ln q_e = \ln k_F + \frac{1}{n} \ln C_e \quad (7)$$

In the equation, c_e is the solution concentration at adsorption equilibrium, in $\text{mg}\cdot\text{L}^{-1}$, q_e is the equilibrium adsorption amount, in $\text{mg}\cdot\text{g}^{-1}$, q_m is the saturated adsorption amount of adsorbate monolayer, in $\text{mg}\cdot\text{g}^{-1}$, k_L is the affinity between adsorbents and adsorbates, in $\text{L}\cdot\text{mg}^{-1}$; k_F is the adsorption equilibrium constant, in $\text{mg}\cdot\text{g}^{-1}$. $\frac{1}{n}$ is the adsorption intensity.

The adsorption thermodynamics were analyzed using the thermodynamic model to solve the standard Gibbs free energy ΔG^0 of adsorption reaction:

$$\Delta G^0 = -RT \ln k_0 \quad (8)$$

$$\ln k_0 = -\frac{\Delta H^0}{RT} + \frac{\Delta S^0}{R} \quad (9)$$

In the equation, ΔG^0 is the Gibbs free energy, in $\text{kJ}\cdot\text{mol}^{-1}$. R is the ideal gas constant, $8.314 \text{ J}\cdot\text{mol}^{-1}\cdot\text{K}^{-1}$. T is the absolute temperature, in K. k_0 is the adsorption equilibrium constant. ΔH^0 is the reaction entropy change, in $\text{kJ}\cdot\text{mol}^{-1}$; ΔS^0 is the reaction enthalpy change, in $\text{J}\cdot\text{mol}^{-1}\text{K}^{-1}$.

Another important characteristic parameter of the Langmuir isothermal adsorption model R_L is a dimensionless parameter similar to the equilibrium constant, which can be used to predict the suitability of adsorption reactions:

$$R_L = \frac{1}{1 + K_L C_0} \quad (10)$$

In the equation, K_L is the Langmuir constant. C_0 is the initial concentration of Pb^{2+} and Cd^{2+} .

In order to investigate the effect of the amount of MHBC on the adsorption of Pb^{2+} and Cd^{2+} in solution, the solid–liquid ratio of MHBC was adjusted to 0.25–2.75 $g \cdot L^{-1}$ (the gradient is 0.50 $g \cdot L^{-1}$).

In order to study the effect of pH on the adsorption of Pb^{2+} and Cd^{2+} in solution, the experiment was carried out by adjusting the initial pH of the solution to 2.0–6.0 (the gradient is 1.0) with a small amount of 0.1 $mol \cdot L^{-1}$ HNO_3 and $NaOH$.

In order to investigate how ionic strength affects the adsorption of Pb^{2+} and Cd^{2+} in solution, the concentration of $NaNO_3$ was adjusted to 0–0.30 $mol \cdot L^{-1}$ (the gradient is 0.05 $mol \cdot L^{-1}$).

In order to research the repeatable utilization rate of MHBC, MHBC after adsorption equilibrium was separated from the ionic solution, washed with deionized water 3 times, and 0.10 $mol \cdot L^{-1}$ HCl was used as the desorption agent to cycle five times of adsorption and desorption.

3. Results and Discussion

3.1. Determination of Optimal MHBC Conditions

As shown in Figure 1, when the initial concentration was 20–500 $mg \cdot L^{-1}$, the MHBC modified by the ratio of 0.3 $mol \cdot L^{-1}$ potassium permanganate and 1 $mol \cdot L^{-1}$ nitric acid always maintained a high adsorption rate of Pb^{2+} and Cd^{2+} in water. There was a tendency for the adsorption rate to decrease with increasing initial and nitric acid concentrations, but there was no significant difference between MH1, MH2, and MH3, indicating that the increase in nitric acid concentration did not significantly promote the adsorption of Pb^{2+} and Cd^{2+} in water; this may be because the high concentration of nitric acid can improve the hydrophobicity of BC [36]. Considering the adsorption effect and cost savings of the material, the best ratio of potassium permanganate and nitric acid was determined to be 0.3: 1.0 $mol \cdot L^{-1}$; this was used to carry out subsequent batch adsorption experiments.

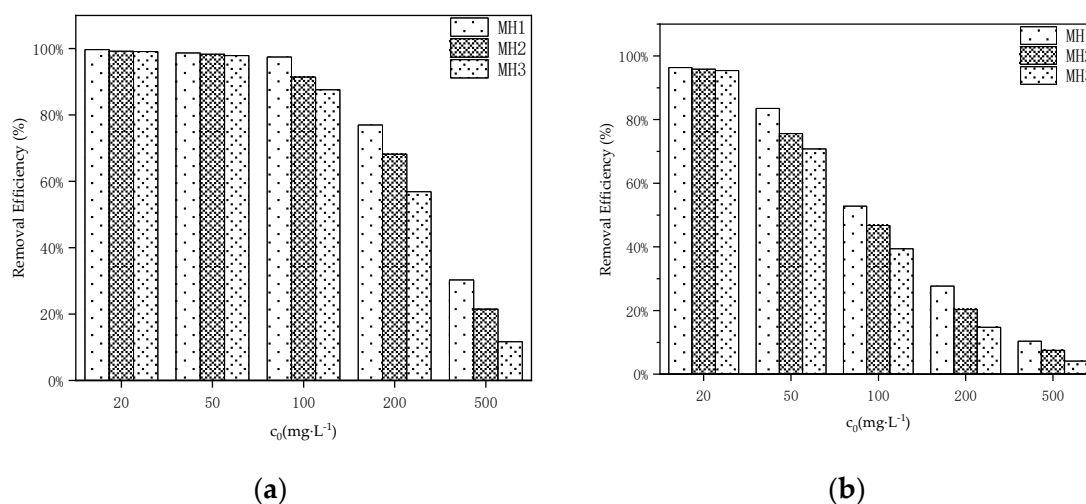


Figure 1. Effect of MHBC with different concentration ratios of potassium permanganate and nitric acid on Pb^{2+} (a) and Cd^{2+} (b) at 25 °C and pH = 5.5.

3.2. Characterization

The SEM images of BC and MHBC were analyzed and compared. As shown in Figure 2, the surface of BC is porous and relatively smooth, which is a common feature of pyrolytic biochar [37,38]. The surface of MHBC is relatively rough and has more irregular ultra-fine particles, which can provide more adsorption sites to improve the adsorption capacity of MHBC.

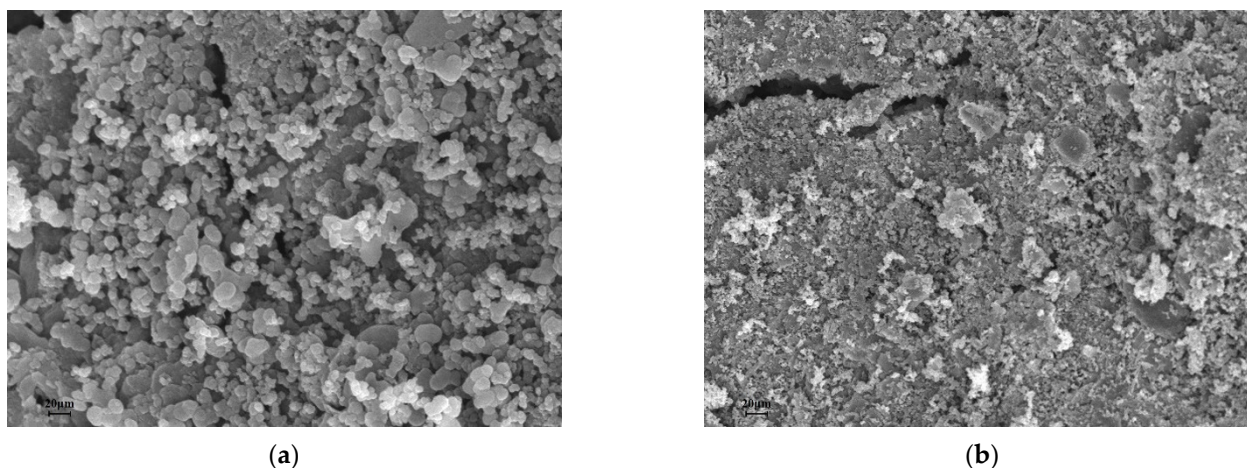


Figure 2. SEM images of BC (a) and MHBC (b).

There are a number of important factors that affect the adsorption energy of MHBC, such as the specific surface area, pore size, and pore volume [39]. As shown in Table 1, the specific surface area of MHBC ($475.36 \text{ m}^2 \cdot \text{g}^{-1}$) increased noticeably, which is 3.02 times the specific surface area of BC ($157.46 \text{ m}^2 \cdot \text{g}^{-1}$), but not higher than $500 \text{ m}^2 \cdot \text{g}^{-1}$, indicating that the main adsorption of MHBC does not depend on pores. The pore volume of MHBC increased, but the pore size decreased, which indicates that the modification not only increases the external area by reducing the pore size, but also improves the internal structure of BC and increases the internal surface area, forming a complex adsorption structure [40,41].

Table 1. Elemental composition and surface morphology parameters of BC and MHBC.

Sample	Pb $\text{mg} \cdot \text{kg}^{-1}$	Cd $\text{mg} \cdot \text{kg}^{-1}$	SBET $\text{m}^2 \cdot \text{g}^{-1}$	Vtot $\text{cm}^3 \cdot \text{g}^{-1}$	Pore Width nm	C	H	O	N
BC	12.37	0.19	157.46	0.21	3.80	77.62	3.91	9.15	0.33
MHBC	12.38	0.18	475.36	0.38	1.65	71.58	3.22	13.37	0.52

H/C and (O + N)/C molar ratios can be used to characterize the aromaticity and polarity of adsorbents. The lower the H/C value, the higher the aromaticity of the material, while a lower (O + N)/C value indicates a higher non-polarity of the material [42–45]. As shown in Table 1, the H/C ratio of modified MHBC decreased, indicating that the aromaticity of BC improved after modification, while the ratios of O/C and (O + N)/C increased, indicating that the polarity of MHBC increased and the oxygen-containing functional groups increased.

It can be seen from Figure 3 that the modification has a significant effect on the oxygen-containing functional groups on the surface of BC. The absorption peak near the wavenumber 3436 cm^{-1} is attributed to the stretching vibration of -OH [46], indicating that the oxygen-containing functional groups, such as hydroxyl groups in the modified MHBC, increased. The absorption peak near the wavenumber of 1627 cm^{-1} is attributed to the residual intermolecular water [47], and the absorption peak near the wavenumbers of 1383 cm^{-1} and 1127 cm^{-1} are the stretching vibrations of various aromatic ethers or O-H and C-O, indicating that the modified MHBC has a good aromatic structure [48]. The appearance of the wavenumber at 2169 cm^{-1} indicates $\text{C} \equiv \text{C}$ stretching vibration [49,50].

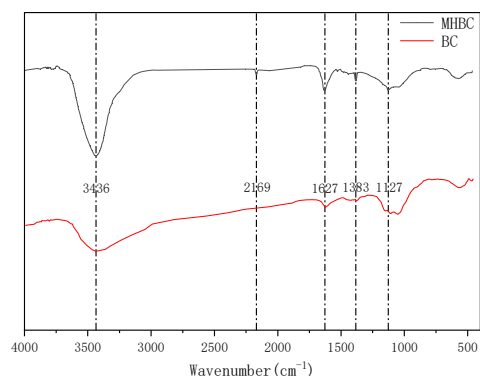


Figure 3. FTIR spectra of BC and MHBC.

The results of the oxygen-containing functional group (OFG) contained in BC and MHBC measured with Boehm titration are shown in Table 2. Compared with BC, the contents of hydroxyl, internal lipid, and carboxyl functional groups in MHBC increased by 0.25, 0.31, and 0.08 mmol·g⁻¹, respectively, which is consistent with the results of the FTIR analysis. The oxygen-containing functional groups on the surface of MHBC are more abundant, and can react better with Pb²⁺ and Cd²⁺. The possible chemical reactions are as follows:

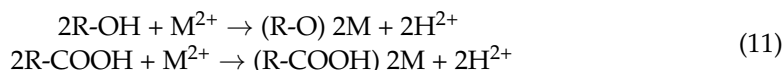


Table 2. Boehm titration results of BC and MHBC.

Sample	Acidic Functional Groups mmol·g ⁻¹	Carboxyl mmol·g ⁻¹	Lactone mmol·g ⁻¹	Phenol mmol·g ⁻¹
BC	0.43	0.11	0.13	0.17
MHBC	1.14	0.36	0.44	0.25

3.3. Optimization of MHBC Dose

As shown in Figure 4, as the solid–liquid ratio of MHBC increased from 0.25 g·L⁻¹ to 2.75 g·L⁻¹; the removal efficiency of Pb²⁺ and Cd²⁺ increased gradually because at a certain initial ion concentration, increasing the use of adsorbents can provide a larger surface area or more adsorption sites, which was similar to most materials for adsorbing pollutants. However, beyond 1.25 g·L⁻¹, the increasing rate of removal rate decreased noticeably. Considering the adsorption effect and cost savings of the materials, the optimum solid–liquid ratio of MHBC was determined to be 1.25 g·L⁻¹, and the follow-up batch adsorption experiments were carried out.

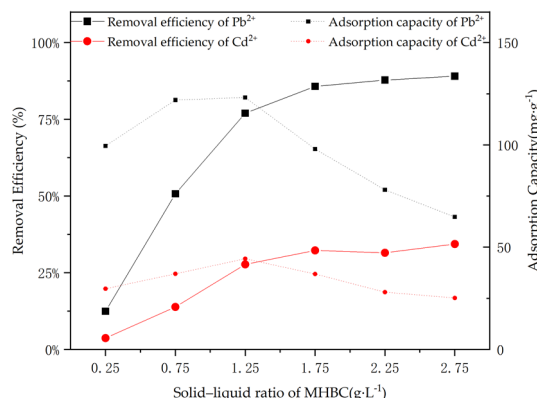


Figure 4. Effect of MHBC dose on Pb²⁺ and Cd²⁺.

3.4. Adsorption Kinetics

The adsorption kinetics curve describes the effects of various factors on the adsorption rate of MHBC. The adsorption kinetics curve of MHBC adsorption of the Pb^{2+} and Cd^{2+} , pseudo-first-order model, the pseudo-second-order model, and the Weber–Morris model were fitted to the adsorption kinetic data of Pb^{2+} and Cd^{2+} , as shown in Figure 5, and the fitting data are shown in Tables 3 and 4. When the ratio of solid to liquid was $1.25 \text{ g}\cdot\text{L}^{-1}$, and the initial $\text{pH} = 5.5$, the initial concentration of the Pb^{2+} and Cd^{2+} solution was $200 \text{ mg}\cdot\text{L}^{-1}$, the adsorption rates of Pb^{2+} and Cd^{2+} on MHBC increased rapidly, then decreased gradually and tended to be stable, in which the adsorption equilibrium of Pb^{2+} was reached at 2 h, and that of Cd^{2+} was reached at 4 h.

Table 3. The pseudo-first-order and the pseudo-second-order kinetics parameters of Pb^{2+} and Cd^{2+} sorption on the MHBC.

Adsorbate	Pseudo-First-Order			Pseudo-Second-Order		
	$q_{e,\text{cal}} \text{ (mg}\cdot\text{g}^{-1}\text{)}$	$k_1 \text{ (h}^{-1}\text{)}$	R^2	$q_{e,\text{cal}} \text{ (mg}\cdot\text{g}^{-1}\text{)}$	$k_2 \text{ (g}\cdot\text{mg}^{-1}\cdot\text{h}^{-1}\text{)}$	R^2
Pb^{2+}	17.90	0.65	0.904	123.92	0.13	0.999
Cd^{2+}	9.13	0.59	0.906	44.80	0.24	0.999

Table 4. The Weber–Morris model kinetics parameters of Pb^{2+} and Cd^{2+} sorption on the MHBC.

Adsorbate	First-Stage			Weber–Morris Second-Stage			Third-Stage		
	C	k	R^2	C	k	R^2	C	k	R^2
Pb^{2+}	56.27	76.54	0.998	103.17	11.68	0.840	121.57	0.49	0.775
Cd^{2+}	16.25	28.94	0.898	33.68	6.14	0.778	44.21	0.01	0.006

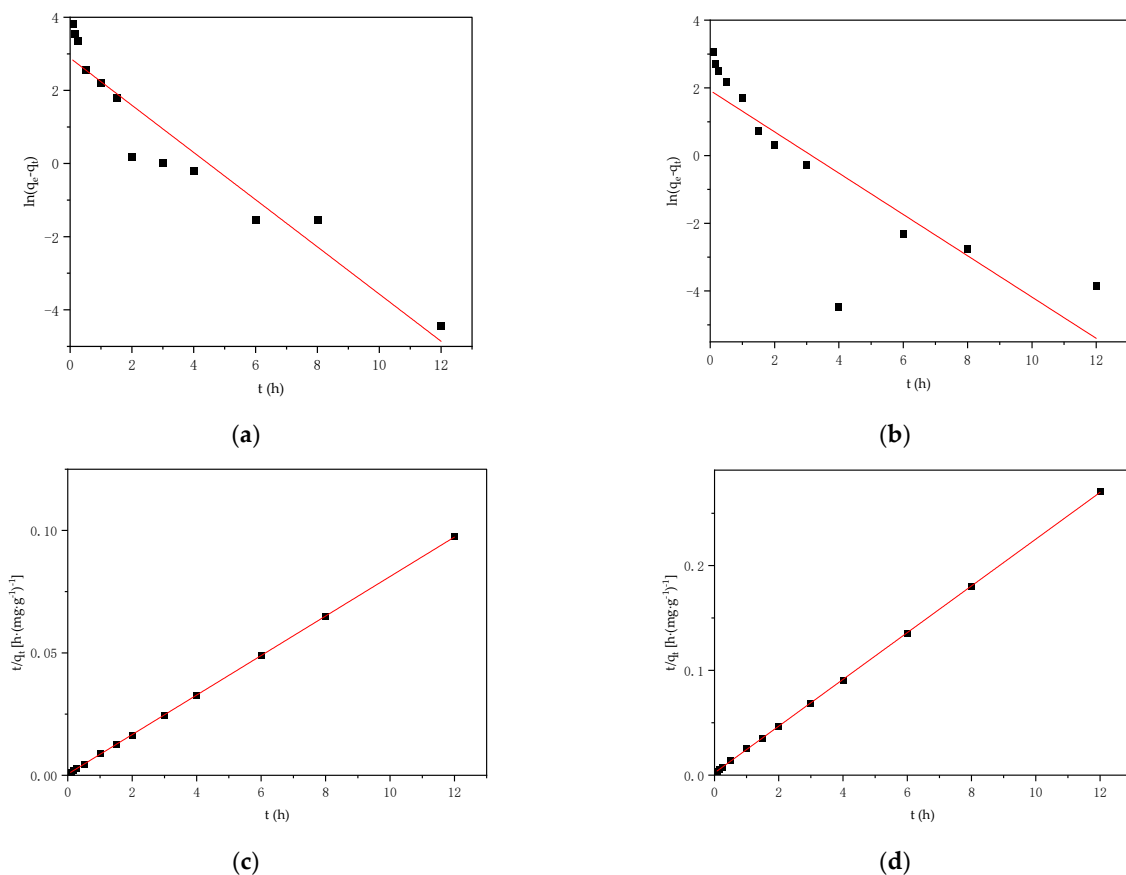


Figure 5. Cont.

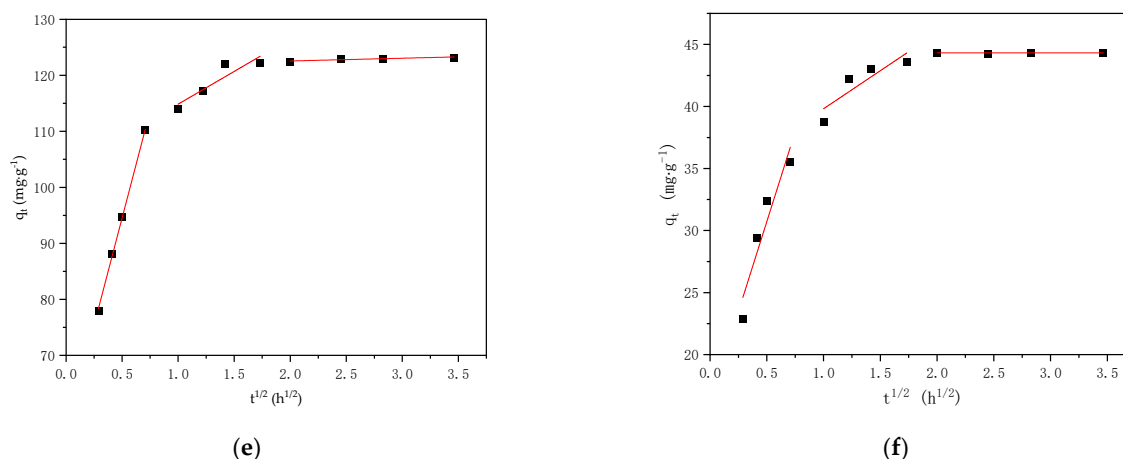


Figure 5. Experimental kinetic data for adsorption of Pb²⁺ and Cd²⁺ by MHBC and their fitting to the kinetic model. (a) Pseudo-first-order model for adsorption of Pb²⁺, (b) pseudo-first-order for adsorption of Cd²⁺, (c) pseudo-second-order model for adsorption of Pb²⁺, (d) pseudo-second-order model for adsorption of Cd²⁺, (e) Weber–Morris model for adsorption of Pb²⁺, (f) Weber–Morris model for adsorption of Cd²⁺.

The pseudo-first-order kinetic model mainly represents an adsorption process controlled by the diffusion motion of boundary molecules, whereas the pseudo-second-order model assumes that the adsorption rate is controlled by chemical mechanisms and considers that there is electron transfer and sharing between adsorbates and adsorbents [51–54]. The correlation coefficient R^2 shows that the best model that fits the adsorption data is the pseudo-second-order kinetic adsorption model (the R^2 of Pb²⁺ and Cd²⁺ is 0.999). The maximum adsorption capacity fitted by the pseudo-second-order kinetic model (123.92 and 44.80 mg·g⁻¹ for Pb²⁺ and Cd²⁺, respectively) is also closer to the experimental results (123.20 and 44.39 mg·g⁻¹ for Pb²⁺ and Cd²⁺, respectively). Therefore, the means of adsorption of the Pb²⁺ and Cd²⁺ solution by MHBC tended to be chemical adsorption [55].

The Weber–Morris model is suitable for the adsorption process with the change in adsorption rate [56]. According to the linear relationship between q_t and $t^{1/2}$, the adsorption of the Pb²⁺ and Cd²⁺ single-system solution by MHBC can be divided into three stages. The initial stage is the external diffusion stage, and there are a large number of adsorption sites on the surface of the MHBC. At the same time, there is a large difference in the ion concentrations between the outer surface and the interior of the MHBC, so Pb²⁺ and Cd²⁺ spread rapidly to the surface of the MHBC and are adsorbed rapidly. The second stage is the intra-particle diffusion stage; the adsorption process begins to spread to the interior of the MHBC and further reacts with the internal active sites of the MHBC, but due to the saturation of surface adsorption and the enhancement of the inward diffusion blocking force, this process is relatively slow. The intra-particle diffusion stage diagram does not pass through the origin, indicating that the adsorption rate is not only affected by intra-particle diffusion. In the later stage, the adsorption gradually tends to equilibrium as ion concentration in the solution decreases [57–59].

3.5. Adsorption Thermodynamics

The isothermal adsorption model is a mathematical model that describes the morphological distribution of adsorbates in solid and liquid phases; it is used to fit the relationship between the ion content on the adsorbent and the equilibrium ion concentration of the solution. The adsorption isotherms of Pb²⁺ and Cd²⁺ on MHBC are L-shaped, indicating that the adsorption is gradually saturated, and MHBC has a limited adsorption capacity. The isotherm data were simulated with the Langmuir and Freundlich models, the results of the fitting parameters are summarized in Tables 5 and 6, and the fitting curve is shown in Figure 6.

Table 5. Isothermal sorption parameters of Pb²⁺ sorption on the MHBC.

T	Langmuir			Freundlich		
	q _{e,cal} (mg·g ⁻¹)	k _L (L·mg ⁻¹)	R ²	k _F	n	R ²
25	124.31	0.73	0.993	53.63	4.17	0.855
35	131.54	0.85	0.990	59.06	4.49	0.833
45	144.29	0.95	0.976	62.06	3.93	0.896
55	160.41	0.98	0.958	68.25	3.81	0.848

Table 6. Isothermal sorption parameters of Cd²⁺ sorption on the MHBC.

Table	Langmuir			Freundlich		
	q _{e,cal} (mg·g ⁻¹)	k _L (L·mg ⁻¹)	R ²	k _F	n	R ²
25	44.37	0.57	0.968	22.82	6.88	0.872
35	45.82	0.65	0.956	23.69	6.88	0.883
45	47.16	0.66	0.953	24.20	6.79	0.886
55	47.46	0.78	0.941	24.39	6.54	0.876

The adsorption constant k_L of the Langmuir model increases with an increase in reaction temperature, showing that the affinity of MHBC adsorbent with Pb²⁺ and Cd²⁺ in solution is higher at high temperature, and it is easier to immobilize free Pb²⁺ and Cd²⁺ by the adsorption reaction. The Freundlich adsorption constant k_F increases sequentially with an increase in temperature, which is consistent with the change in the Langmuir model adsorption constant k_L ; that is, higher temperatures help the adsorption reaction to take place. The n value reflects the intensity of the adsorption reaction, and the n value is in the range of 3.807–6.878, and $\frac{1}{n}$ is less than 1, showing that the adsorption of Pb²⁺ and Cd²⁺ is an ideal adsorption process that easily occurs [60,61].

In the range of 25–55 °C, the correlation coefficients of the Langmuir isotherms fitting (R² of Pb²⁺ and Cd²⁺ = 0.958–0.993 and 0.941–0.968) are more accurate than those of the Freundlich isotherms (R² of Pb²⁺ and Cd²⁺ = 0.833–0.896 and 0.872–0.886), which indicates that the Langmuir isotherms can better describe the adsorption of Pb²⁺ and Cd²⁺ by MHBC. The adsorption of Pb²⁺ and Cd²⁺ is a single chemical adsorption layer on the surface of the adsorbents with uniform adsorption sites [62–64].

In this study, the R_L (0.42–0.88) of Pb²⁺ and the R_L (0.24–0.75) of Cd²⁺ were between 0 and 1, which further indicates that the adsorption of Pb²⁺ and Cd²⁺ is a suitable process [65].

The isothermal adsorption experiments show that a change in temperature will significantly affect the adsorption process of Pb²⁺ and Cd²⁺ by MHBC. Each thermodynamic parameter is closely linked to the practical application of the adsorption process, characterizing the change in energy internal to the adsorbent and the product in the reaction process. The change during the reaction is important evidence that reveals whether the adsorption process is spontaneous or not. Table 6 shows the ΔG^0 of the adsorption reaction calculated according to the equilibrium adsorption constant k_L of the Langmuir isothermal adsorption model at different reaction temperatures.

Table 7 shows the ΔG^0 of the adsorption reaction calculated according to the equilibrium adsorption constant k_L of the Langmuir isothermal adsorption model at different reaction temperatures. ΔG^0 is negative, indicating that the adsorption process is spontaneous. With an increase in temperature, ΔG^0 decreases, indicating a stronger adsorption capacity. The enthalpy change ΔH^0 of the reaction is positive, indicating that the adsorption process is an endothermic reaction, and an increase in temperature increases the voids or active sites on the surface of the adsorbent, thus promoting rapid occurrence of the adsorption process [65–67]. Through the results, it was proven that the adsorption characteristic constant k_L of Langmuir model, the adsorption constant k_F of Freundlich model, and the adsorption capacity increased with increasing reaction temperature. In terms of the adsorption kinetics, Pb²⁺ and Cd²⁺ have almost the same charge, but the adsorption rate of Pb²⁺ is twice as fast as that of Cd²⁺. This is probably due to the higher enthalpy of Pb²⁺, which increases its chemical adsorption rate, while that of Cd²⁺ is relatively weak.

The positive value of the entropy change ΔS^0 also proved there was an increase in the percentage of free active sites on the solid–liquid reaction interface during the adsorption of Pb^{2+} and Cd^{2+} by MHBC [61,65,68].

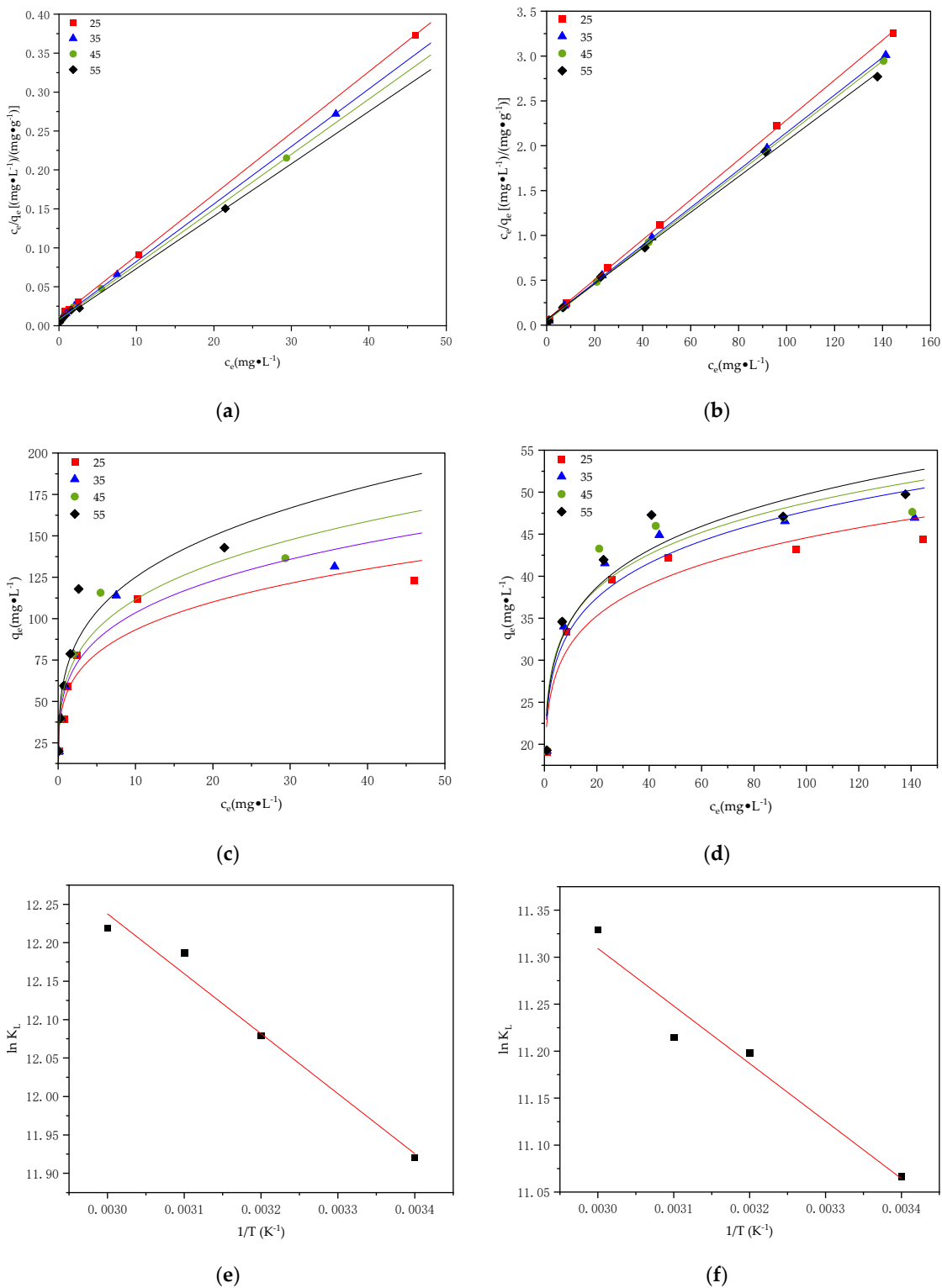


Figure 6. Experimental isotherm data of Pb^{2+} and Cd^{2+} uptake by MHBC and their fit to the Langmuir model and the Freundlich model: Langmuir model for adsorption of Pb^{2+} (a) and Cd^{2+} (b), Freundlich model for adsorption of Pb^{2+} (c) and Cd^{2+} (d), thermodynamic parameter fitting for adsorption of Pb^{2+} (e) and Cd^{2+} (f).

Table 7. Thermodynamic parameters of Pb^{2+} and Cd^{2+} sorption onto the MHBC.

	Temp k	k_L	ΔG^0 $\text{kJ}\cdot\text{mol}^{-1}$	ΔH^0 $\text{kJ}\cdot\text{mol}^{-1}$	ΔS^0 $\text{kJ}\cdot\text{mol}^{-1}$
Pb^{2+}	298	150,273.72	−29.53	6.485	121.20
	308	176,132.16	−30.93		
	318	196,169.76	−32.22		
	328	202,551.57	−33.32		
	298	64,027.04	−27.42		
Cd^{2+}	308	73,009.44	−28.68	5.092	109.30
	318	74,180.96	−29.65		
	328	83,195.84	−30.89		

3.6. pH

The pH value of the solution will affect the surface functional groups, charge, and metal ion morphology of the adsorbent, and then affect the ion exchange and precipitation reaction [69]. Figure 7 shows that the initial pH significantly affects the adsorption of Pb^{2+} and Cd^{2+} by MHBC. As shown in Figure 7, with an increase in pH, the adsorption capacity of MHBC to Pb^{2+} and Cd^{2+} increases gradually, and when the initial pH value is lower than 3.5, the adsorption capacity of Pb^{2+} and Cd^{2+} is relatively low, which may be due to the fact that at low pH values, a large number of H_3O^+ and H^+ occupy the adsorption sites on the MHBC surface, making H_3O^+ and H^+ adsorption competitors [70,71].

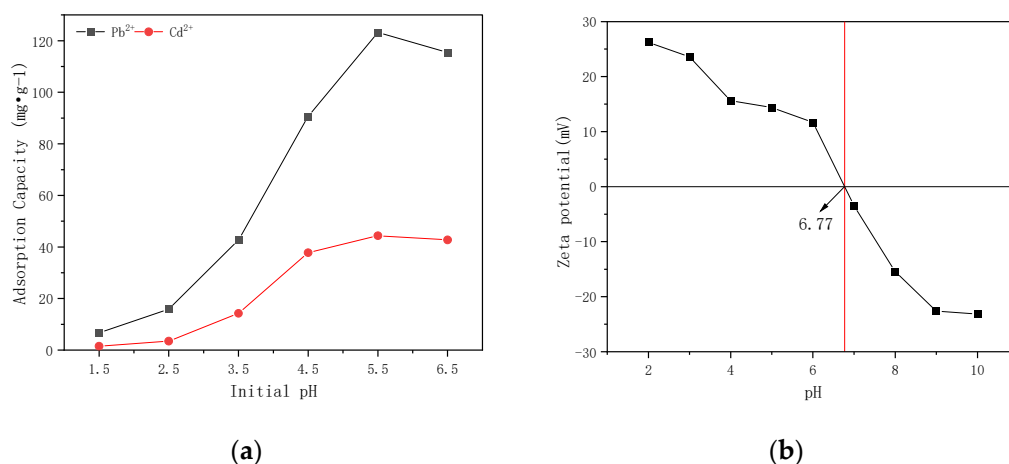


Figure 7. (a) Effect of initial pH on Pb^{2+} and Cd^{2+} adsorption for MHBC. (b) The relationship between zeta potential and pH value of MHBC.

With an increase in the pH value (pH = 3.5–5.5), the competitive adsorption of H_3O^+ and H^+ decreased, and consequently the adsorption capacity of MHBC for Pb^{2+} and Cd^{2+} increased sharply; the adsorption capacities increased from $42.73 \text{ mg}\cdot\text{g}^{-1}$ to $123.18 \text{ mg}\cdot\text{g}^{-1}$ and $14.27 \text{ mg}\cdot\text{g}^{-1}$ to $44.39 \text{ mg}\cdot\text{g}^{-1}$, respectively. When the pH is greater than 6.5, Pb^{2+} and Cd^{2+} exist mainly in the form of hydroxide, so there is no weak alkali environment in this experiment, and many researchers have come to the same conclusion in the adsorption experiments of Pb^{2+} and Cd^{2+} [21,24,48,64,72,73].

The zeta potential value can describe the effect of pH on Pb^{2+} and Cd^{2+} adsorption. Figure 7 shows that the zeta potential value of MHBC is 6.77. During the adsorption process, the zeta of MHBC is higher than the optimal pH of the Pb^{2+} and Cd^{2+} solution (pH = 5.5), which means that the surface of the MHBC is always positively charged and will electrostatically repel the positively charged Pb^{2+} and Cd^{2+} ; however, MHBC has a high affinity for Pb^{2+} and Cd^{2+} , indicating that electrostatic attraction may not be the main adsorption mechanism, and that the main adsorption mechanism should be a chemical process [74,75].

3.7. Coexisting Ion

The existence of cations may affect the adsorption capacity of the materials. In order to investigate the effect of co-cations on the adsorption equilibrium of Pb^{2+} and Cd^{2+} , the batch adsorption of K^+ , Na^+ , Ca^{2+} , and the Pb^{2+} and Cd^{2+} was performed.

As shown in Figure 8, the adsorption capacity of MHBC on Pb^{2+} and Cd^{2+} decreased as the concentrations of K^+ and Na^+ increased from $0.01 \text{ mol}\cdot\text{L}^{-1}$ to $5 \text{ mol}\cdot\text{L}^{-1}$, but the changes were not significant, indicating that there was no obvious competition between K^+ and Na^+ on the adsorption of Pb^{2+} and Cd^{2+} on the adsorbent surface. The adsorption capacity of MHBC on Pb^{2+} and Cd^{2+} was not affected by K^+ and Na^+ .

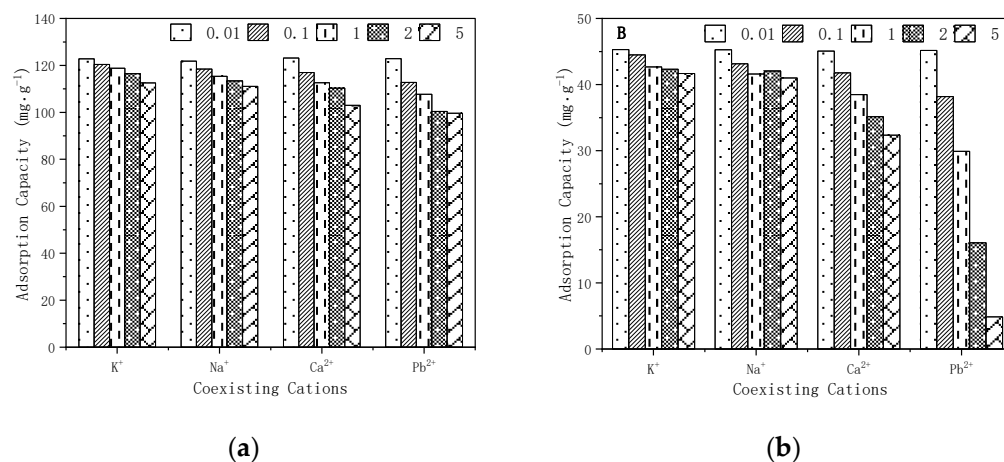


Figure 8. Effect of coexisting cations on Pb^{2+} (a) and Cd^{2+} (b) adsorption for MHBC.

When the concentration of Ca^{2+} exceeded $1 \text{ mol}\cdot\text{L}^{-1}$, the adsorption capacity of MHBC on Pb^{2+} did not change significantly, but significantly affected the adsorption capacity of MHBC on Cd^{2+} ; the adsorption capacity decreased from $45.36 \text{ mg}\cdot\text{g}^{-1}$ to $38.47 \text{ mg}\cdot\text{g}^{-1}$, which may be due to the weak covalent nature of Ca^{2+} , resulting in lower hydration of Ca^{2+} and easier adsorption on the MHBC surface [76].

When Pb^{2+} and Cd^{2+} coexisted, an increase in the concentration of Cd^{2+} had no significant effect on the adsorption of Pb^{2+} , but with an increase in the concentration of Pb^{2+} , the adsorption of Cd^{2+} decreased from $45.36 \text{ mg}\cdot\text{g}^{-1}$ to $4.85 \text{ mg}\cdot\text{g}^{-1}$, which decreased by 89.31%; this indicates that there was clear competition between Pb^{2+} and Cd^{2+} for adsorption, and Pb^{2+} had a significant competitive advantage. This may be due to the higher affinity of the hydroxyl and carboxyl groups for Pb^{2+} in the adsorbent [77], and that Pb^{2+} has a smaller hydration radius and lower $\text{p}K_{\text{H}}$ (negative log of hydrolysis constant) than Cd^{2+} . Therefore, Pb^{2+} is more readily adsorbed by MHBC through surface complexation or adsorption reactions in ion-interference environments [78].

3.8. Reuse

The cycling performance of an adsorbent is very important for practical applications. In order to evaluate the stability of the adsorption capacity of MHBC for Pb^{2+} and Cd^{2+} , five cycles of adsorption experiments were performed. As shown in Figure 9, the adsorption capacity of MHBC for Pb^{2+} and Cd^{2+} decreased with an increasing number of cycles, which is probably due to the structural degradation of the adsorbent and the loss of surface minerals [79]. After the fifth cycle, the adsorption capacities of MHBC for Pb^{2+} and Cd^{2+} reached $106.31 \text{ mg}\cdot\text{g}^{-1}$ and $39.67 \text{ mg}\cdot\text{g}^{-1}$, respectively, which were 88.57% and 85.15% of the initial adsorption capacities, respectively. The results showed that MHBC has good reusability.

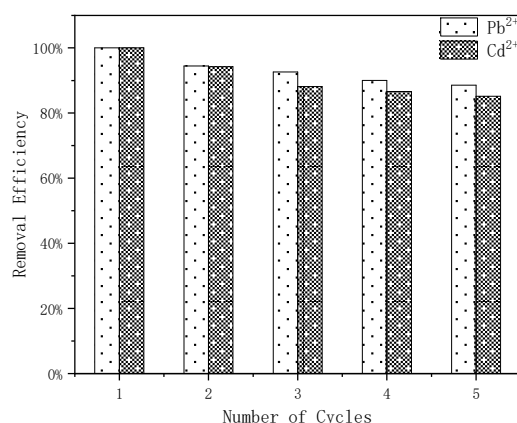


Figure 9. Pb (II) and Cd (II) adsorption–desorption recycle performance.

4. Conclusions

In this study, we prepared MHBC, using potassium permanganate and nitric acid, in order to evaluate the removal capacity of MHBC for Pb²⁺ and Cd²⁺ in a single aqueous environment through batch tests. The characterization analysis showed that the MHBC had an increased specific surface, enhanced polarity, and rich oxygen-containing functional groups, which can provide more adsorption sites to improve the adsorption capacity. The adsorption kinetic data showed that Pb²⁺ and Cd²⁺ were rapidly adsorbed by MHBC within 1 h, and reached their adsorption equilibria after 2 h and 4 h, respectively. The adsorption thermodynamic adsorption data showed that the adsorption of Pb²⁺ and Cd²⁺ by MHBC was monolayer adsorption, which was a spontaneous heat absorption reaction; the higher the temperature, the stronger the adsorption capacity. The maximum adsorption of the Pb²⁺ and Cd²⁺ by MHBC reached 160.41 mg·g⁻¹ and 47.46 mg·g⁻¹ at pH = 5.5 and 55 °C, respectively, which had obvious adsorption advantages compared with other adsorption materials [13,14,26,30,51,57,62,78]. The coexistence of K⁺, Na⁺, Ca²⁺, and Cd²⁺ showed no significant change in the adsorption of Pb²⁺ by MHBC. However, the adsorption of MHBC on Cd²⁺ was significantly decreased in the presence of Ca²⁺ and Pb²⁺. After five cycles of adsorption analysis, the adsorption amounts of MHBC for Pb²⁺ and Cd²⁺ remained at more than 85% of the initial adsorption amounts. MHBC is an economical and green recyclable adsorption material, which can effectively expand its application potential in agricultural water environmental pollution treatment.

Author Contributions: Conceptualization, H.Q. and X.S.; methodology, H.Q. and X.S.; software, H.Q.; validation, H.Q., X.S. and W.G.; investigation, H.Q., X.S., H.S. and W.G.; data curation, H.Q.; writing—original draft preparation, H.Q. and X.S.; writing—review and editing, H.Q., X.S., H.S., W.G. and Y.A.H.; supervision, X.S.; funding acquisition, X.S. All authors have read and agreed to the published version of the manuscript.

Funding: This research was funded by the Jiangsu Province Science and Technology Plan Project (grant number BE2015705).

Data Availability Statement: Not applicable.

Conflicts of Interest: The authors declare no conflict of interest.

References

1. Briffa, J.; Sinagra, E.; Blundell, R. Heavy metal pollution in the environment and their toxicological effects on humans. *Heliyon* **2020**, *6*, 26. [CrossRef]
2. Zhong, T.Y.; Xue, D.W.; Zhao, L.M.; Zhang, X.Y. Concentration of heavy metals in vegetables and potential health risk assessment in China. *Environ. Geochem. Health* **2018**, *40*, 313–322. [CrossRef] [PubMed]
3. Wang, L.K.; Mao, X.Y.; Hamoud, Y.A.; Zhu, N.Y.; Shao, X.H.; Wang, Q.L.; Shaghaleh, H. Nitrogen Removal for Low Concentration Ammonium Wastewater by Adsorption, Shortcut Simultaneous Nitrification and Denitrification Process in MBBR. *Water* **2023**, *15*, 1334. [CrossRef]

4. Wang, L.K.; Zhu, N.Y.; Shaghaleh, H.; Mao, X.Y.; Shao, X.H.; Wang, Q.L.; Hamoud, Y.A. The Effect of Functional Ceramsite in a Moving Bed Biofilm Reactor and Its Ammonium Nitrogen Adsorption Mechanism. *Water* **2023**, *15*, 1362. [[CrossRef](#)]
5. Li, Z.Y.; Ma, Z.W.; van der Kuip, T.J.; Yuan, Z.W.; Huang, L. A review of soil heavy metal pollution from mines in China: Pollution and health risk assessment. *Sci. Total Environ.* **2014**, *468*, 843–853. [[CrossRef](#)]
6. Burakov, A.E.; Galunin, E.V.; Burakova, I.V.; Kucherova, A.E.; Agarwal, S.; Tkachev, A.G.; Gupta, V.K. Adsorption of heavy metals on conventional and nanostructured materials for wastewater treatment purposes: A review. *Ecotoxicol. Environ. Saf.* **2018**, *148*, 702–712. [[CrossRef](#)] [[PubMed](#)]
7. Harvey, P.J.; Handley, H.K.; Taylor, M.P. Identification of the sources of metal (lead) contamination in drinking waters in north-eastern Tasmania using lead isotopic compositions. *Environ. Sci. Pollut. Res.* **2015**, *22*, 12276–12288. [[CrossRef](#)]
8. Zhu, W.; Wang, J.; Wu, D.; Li, X.; Luo, Y.; Han, C.; Ma, W.; He, S. Investigating the Heavy Metal Adsorption of Mesoporous Silica Materials Prepared by Microwave Synthesis. *Nanoscale Res. Lett.* **2017**, *12*, 323. [[CrossRef](#)]
9. Mao, X.Y.; Sun, J.J.; Shaghaleh, H.; Jiang, X.S.; Yu, H.Z.; Zhai, S.M.; Hamoud, Y.A. Environmental Assessment of Soils and Crops Based on Heavy Metal Risk Analysis in Southeastern China. *Agronomy* **2023**, *13*, 1107. [[CrossRef](#)]
10. Gopinathan, R.; Bhowal, A.; Garlapati, C. Adsorption Characteristics of Activated Carbon for the Reclamation of Colored Effluents Containing Orange G and New Solid-Liquid Phase Equilibrium Model. *J. Chem. Eng. Data* **2017**, *62*, 558–567. [[CrossRef](#)]
11. Grotzner, M.; Melchior, E.; Schroeder, L.H.; dos Santos, A.R.; Moscon, K.G.; de Andrade, M.A.; Martinelli, S.H.S.; Xavier, C.R. Pulp and Paper Mill Effluent Treated by Combining Coagulation-Flocculation-Sedimentation and Fenton Processes. *Water Air Soil Pollut.* **2018**, *229*, 7. [[CrossRef](#)]
12. Jaafarzadeh, N.; Baboli, Z.; Noorimotlagh, Z.; Martinez, S.S.; Ahmadi, M.; Alavi, S.; Mirzaee, S.A. Efficient adsorption of bisphenol A from aqueous solutions using low-cost activated carbons produced from natural and synthetic carbonaceous materials. *Desalination Water Treat.* **2019**, *154*, 177–187. [[CrossRef](#)]
13. Karnib, M.; Kabbani, A.; Holail, H.; Olama, Z. Heavy Metals Removal Using Activated Carbon, Silica and Silica Activated Carbon Composite. *Energy Procedia* **2014**, *50*, 113–120. [[CrossRef](#)]
14. Fan, Z.; Zhang, Q.; Li, M.; Niu, D.; Sang, W.; Verpoort, F. Investigating the sorption behavior of cadmium from aqueous solution by potassium permanganate-modified biochar: Quantify mechanism and evaluate the modification method. *Environ. Sci. Pollut. Res.* **2018**, *25*, 8330–8339. [[CrossRef](#)] [[PubMed](#)]
15. Dewage, N.B.; Fowler, R.E.; Pittman, C.U.; Mohan, D.; Mlsna, T. Lead (Pb²⁺) sorptive removal using chitosan-modified biochar: Batch and fixed-bed studies. *RSC Adv.* **2018**, *8*, 25368–25377. [[CrossRef](#)]
16. Dong, L.H.; Liu, W.J.; Jiang, R.F.; Wang, Z.S. Study on the adsorption mechanism of activated carbon removing low concentrations of heavy metals. *Desalination Water Treat.* **2016**, *57*, 7812–7822. [[CrossRef](#)]
17. Han, Y.T.; Cao, X.; Ouyang, X.; Sohi, S.P.; Chen, J.W. Adsorption kinetics of magnetic biochar derived from peanut hull on removal of Cr (VI) from aqueous solution: Effects of production conditions and particle size. *Chemosphere* **2016**, *145*, 336–341. [[CrossRef](#)]
18. Tomczyk, A.; Sokolowska, Z.; Boguta, P. Biochar physicochemical properties: Pyrolysis temperature and feedstock kind effects. *Rev. Environ. Sci. Bio. Technol.* **2020**, *19*, 191–215. [[CrossRef](#)]
19. Doumer, M.E.; Rigol, A.; Vidal, M.; Mangrich, A.S. Removal of Cd, Cu, Pb, and Zn from aqueous solutions by biochars. *Environ. Sci. Pollut. Res.* **2016**, *23*, 2684–2692. [[CrossRef](#)]
20. Park, J.H.; Ok, Y.S.; Kim, S.H.; Cho, J.S.; Heo, J.S.; Delaune, R.D.; Seo, D.C. Competitive adsorption of heavy metals onto sesame straw biochar in aqueous solutions. *Chemosphere* **2016**, *142*, 77–83. [[CrossRef](#)]
21. Wang, Y.Y.; Liu, Y.X.; Lu, H.H.; Yang, R.Q.; Yang, S.M. Competitive adsorption of Pb(II), Cu(II), and Zn(II) ions onto hydroxyapatite-biochar nanocomposite in aqueous solutions. *J. Solid State Chem.* **2018**, *261*, 53–61. [[CrossRef](#)]
22. Lu, S.; Zong, Y. Pore structure and environmental serves of biochars derived from different feedstocks and pyrolysis conditions. *Environ. Sci. Pollut. Res.* **2018**, *25*, 30401–30409. [[CrossRef](#)]
23. Kalina, M.; Sovova, S.; Svec, J.; Trudicova, M.; Hajzler, J.; Kubikova, L.; Enev, V. The Effect of Pyrolysis Temperature and the Source Biomass on the Properties of Biochar Produced for the Agronomical Applications as the Soil Conditioner. *Materials* **2022**, *15*, 8855. [[CrossRef](#)]
24. Peng, H.B.; Gao, P.; Chu, G.; Pan, B.; Peng, J.H.; Xing, B.S. Enhanced adsorption of Cu(II) and Cd(II) by phosphoric acid-modified biochars. *Environ. Pollut.* **2017**, *229*, 846–853. [[CrossRef](#)]
25. Nicola, R.; Costisor, O.; Ciopec, M.; Negrea, A.; Lazau, R.; Ianasi, C.; Piciorus, E.M.; Len, A.; Almasly, L.; Szerb, E.I.; et al. Silica-Coated Magnetic Nanocomposites for Pb²⁺ Removal from Aqueous Solution. *Appl. Sci.* **2020**, *10*, 2726. [[CrossRef](#)]
26. Wongrod, S.; Simon, S.; Guibaud, G.; Lens, P.N.L.; Pechaud, Y.; Huguenot, D.; van Hullebusch, E.D. Lead sorption by biochar produced from digestates: Consequences of chemical modification and washing. *J. Environ. Manag.* **2018**, *219*, 277–284. [[CrossRef](#)] [[PubMed](#)]
27. Ianasi, C.; Piciorus, M.; Nicola, R.; Ciopec, M.; Negrea, A.; Niznansky, D.; Len, A.; Almasly, L.; Putz, A.M. Removal of cadmium from aqueous solutions using inorganic porous nanocomposites. *Korean J. Chem. Eng.* **2019**, *36*, 688–700. [[CrossRef](#)]
28. Li, N.; Yin, M.L.; Tsang, D.C.W.; Yang, S.T.; Liu, J.; Li, X.; Song, G.; Wang, J. Mechanisms of U(VI) removal by biochar derived from *Ficus microcarpa* aerial root: A comparison between raw and modified biochar. *Sci. Total Environ.* **2019**, *697*, 134115. [[CrossRef](#)]
29. Salam, M.A.; Owija, N.Y.; Kosa, S. Removal of the toxic cadmium ions from aqueous solutions by zero-valent iron nanoparticles. *Int. J. Environ. Sci. Technol.* **2021**, *18*, 2391–2404. [[CrossRef](#)]

30. El-Banna, M.F.; Mosa, A.; Gao, B.; Yin, X.Q.; Wang, H.Y.; Ahmad, Z. Scavenging effect of oxidized biochar against the phytotoxicity of lead ions on hydroponically grown chicory: An anatomical and ultrastructural investigation. *Ecotoxicol. Environ. Saf.* **2019**, *170*, 363–374. [[CrossRef](#)]
31. Boyuan, Y.A.O.; Zhifeng, D.O.U.; Guangmin, H.; Rencheng, L.I.U. Pyrolysis and pyrolysis kinetics of coconut shell, coconut shell residue and de-ashed coconut shell residue. *J. Chem. Ind. Eng.* **2007**, *58*, 1210–1214.
32. Samsudin, M.H.; Hassan, M.A.; Idris, J.; Ramli, N.; Mohd Yusoff, M.Z.; Ibrahim, I.; Othman, M.R.; Mohd Ali, A.A.; Shirai, Y. A one-step self-sustained low temperature carbonization of coconut shell biomass produced a high specific surface area biochar-derived nano-adsorbent. *Waste Manag. Res.* **2019**, *37*, 551–555. [[CrossRef](#)] [[PubMed](#)]
33. Kamran, U.; Park, S.J. MnO₂-decorated biochar composites of coconut shell and rice husk: An efficient lithium ions adsorption-desorption performance in aqueous media. *Chemosphere* **2020**, *260*, 15. [[CrossRef](#)] [[PubMed](#)]
34. Liu, H.K.; Xu, F.; Xie, Y.L.; Wang, C.; Zhang, A.K.; Li, L.L.; Xu, H. Effect of modified coconut shell biochar on availability of heavy metals and biochemical characteristics of soil in multiple heavy metals contaminated soil. *Sci. Total Environ.* **2018**, *645*, 702–709. [[CrossRef](#)] [[PubMed](#)]
35. Wu, W.D.; Li, J.H.; Lan, T.; Muller, K.; Niazi, N.K.; Chen, X.; Xu, S.; Zheng, L.R.; Chu, Y.C.; Li, J.W.; et al. Unraveling sorption of lead in aqueous solutions by chemically modified biochar derived from coconut fiber: A microscopic and spectroscopic investigation. *Sci. Total Environ.* **2017**, *576*, 766–774. [[CrossRef](#)]
36. Wang, Y.R.; Zhang, Z.M.; Zhang, S.; Wang, Y.; Hu, S.; Xiang, J.; Hu, X. Steam reforming of acetic acid over Ni/biochar catalyst treated with HNO₃: Impacts of the treatment on surface properties and catalytic behaviors. *Fuel* **2020**, *278*, 14. [[CrossRef](#)]
37. Zheng, H.; Zhang, C.; Liu, B.; Liu, G.; Xing, B. *A New Paradigm for Environmental Chemistry and Toxicology*; Jiang, G.B., Ed.; Springer: Singapore, 2019; pp. 153–196.
38. Ajeng, A.A.; Abdullah, R.; Ling, T.C.; Ismail, S.; Lau, B.F.; Ong, H.C.; Chew, K.W.; Show, P.L.; Chang, J.S. Bioformulation of biochar as a potential inoculant carrier for sustainable agriculture. *Environ. Technol. Innov.* **2020**, *20*, 22. [[CrossRef](#)]
39. Tanhaei, B.; Ayati, A.; Lahtinen, M.; Sillanpaa, M. Preparation and characterization of a novel chitosan/Al₂O₃/magnetite nanoparticles composite adsorbent for kinetic, thermodynamic and isotherm studies of Methyl Orange adsorption. *Chem. Eng. J.* **2015**, *259*, 1–10. [[CrossRef](#)]
40. Zhou, X.J.; Li, X.D.; Xu, S.X.; Zhao, X.Y.; Ni, M.J.; Cen, K.F. Comparison of adsorption behavior of PCDD/Fs on carbon nanotubes and activated carbons in a bench-scale dioxin generating system. *Environ. Sci. Pollut. Res.* **2015**, *22*, 10463–10470. [[CrossRef](#)]
41. Li, Y.Q.; Li, K.X.; Sun, G.H.; Wang, J.L. Synthesis and characterization of activated carbon with a high mesoporosity. *New Carbon Mater.* **2011**, *26*, 130–136. [[CrossRef](#)]
42. Chen, B.L.; Zhou, D.D.; Zhu, L.Z. Transitional adsorption and partition of nonpolar and polar aromatic contaminants by biochars of pine needles with different pyrolytic temperatures. *Environ. Sci. Technol.* **2008**, *42*, 5137–5143. [[CrossRef](#)]
43. Cantrell, K.B.; Hunt, P.G.; Uchimiya, M.; Novak, J.M.; Ro, K.S. Impact of pyrolysis temperature and manure source on physico-chemical characteristics of biochar. *Bioresour. Technol.* **2012**, *107*, 419–428. [[CrossRef](#)]
44. Keiluweit, M.; Nico, P.S.; Johnson, M.G.; Kleber, M. Dynamic Molecular Structure of Plant Biomass-Derived Black Carbon (Biochar). *Environ. Sci. Technol.* **2010**, *44*, 1247–1253. [[CrossRef](#)]
45. Chen, B.L.; Johnson, E.J.; Chefetz, B.; Zhu, L.Z.; Xing, B.S. Sorption of polar and nonpolar aromatic organic contaminants by plant cuticular materials: Role of polarity and accessibility. *Environ. Sci. Technol.* **2005**, *39*, 6138–6146. [[CrossRef](#)]
46. Chen, Y.L.; Pan, B.C.; Li, H.Y.; Zhang, W.M.; Lv, L.; Wu, J. Selective Removal of Cu(II) Ions by Using Cation-exchange Resin-Supported Polyethyleneimine (PEI) Nanoclusters. *Environ. Sci. Technol.* **2010**, *44*, 3508–3513. [[CrossRef](#)] [[PubMed](#)]
47. Rahman, I.A.; Jafarzadeh, M.; Sipaut, C.S. Synthesis of organo-functionalized nanosilica via a co-condensation modification using gamma-aminopropyltriethoxysilane (APTES). *Ceram. Int.* **2009**, *35*, 1883–1888. [[CrossRef](#)]
48. Li, B.; Yang, L.; Wang, C.Q.; Zhang, Q.P.; Liu, Q.C.; Li, Y.D.; Xiao, R. Adsorption of Cd(II) from aqueous solutions by rape straw biochar derived from different modification processes. *Chemosphere* **2017**, *175*, 332–340. [[CrossRef](#)] [[PubMed](#)]
49. Mohan, D.; Pittman, C.U.; Bricka, M.; Smith, F.; Yancey, B.; Mohammad, J.; Steele, P.H.; Alexandre-Franco, M.F.; Gomez-Serrano, V.; Gong, H. Sorption of arsenic, cadmium, and lead by chars produced from fast pyrolysis of wood and bark during bio-oil production. *J. Colloid Interface Sci.* **2007**, *310*, 57–73. [[CrossRef](#)]
50. Jiang, T.Y.; Jiang, J.; Xu, R.K.; Li, Z. Adsorption of Pb(II) on variable charge soils amended with rice-straw derived biochar. *Chemosphere* **2012**, *89*, 249–256. [[CrossRef](#)]
51. Trakal, L.; Veselska, V.; Safarik, I.; Vitkova, M.; Cihalova, S.; Komarek, M. Lead and cadmium sorption mechanisms on magnetically modified biochars. *Bioresour. Technol.* **2016**, *203*, 318–324. [[CrossRef](#)]
52. Lyu, H.H.; Tang, J.C.; Huang, Y.; Gai, L.S.; Zeng, E.Y.; Liber, K.; Gong, Y.Y. Removal of hexavalent chromium from aqueous solutions by a novel biochar supported nanoscale iron sulfide composite. *Chem. Eng. J.* **2017**, *322*, 516–524. [[CrossRef](#)]
53. Ho, Y.S.; McKay, G. Pseudo-second order model for sorption processes. *Process Biochem.* **1999**, *34*, 451–465. [[CrossRef](#)]
54. Ho, Y.S.; McKay, G. Kinetic models for the sorption of dye from aqueous solution by wood. *Process Saf. Environ. Protect.* **1998**, *76*, 183–191. [[CrossRef](#)]
55. Cui, X.Q.; Fang, S.Y.; Yao, Y.Q.; Li, T.Q.; Ni, Q.J.; Yang, X.E.; He, Z.L. Potential mechanisms of cadmium removal from aqueous solution by Canna indica derived biochar. *Sci. Total Environ.* **2016**, *562*, 517–525. [[CrossRef](#)]
56. Kapica, J.; Pelech, R.; Przepiorski, J.; Morawski, A.W. Kinetics of the adsorption of copper and lead ions from aqueous solution on to WD-ekstra activated carbon. *Adsorpt. Sci. Technol.* **2002**, *20*, 441–452. [[CrossRef](#)]

57. Masoumi, A.; Ghaemy, M.; Bakht, A.N. Removal of Metal Ions from Water Using Poly(MMA-co-MA)/Modified-Fe₃O₄ Magnetic Nanocomposite: Isotherm and Kinetic Study. *Ind. Eng. Chem. Res.* **2014**, *53*, 8188–8197. [[CrossRef](#)]
58. Loganathan, P.; Shim, W.G.; Sounthararajah, D.P.; Kalaruban, M.; Nur, T.; Vigneswaran, S. Modelling equilibrium adsorption of single, binary, and ternary combinations of Cu, Pb, and Zn onto granular activated carbon. *Environ. Sci. Pollut. Res.* **2018**, *25*, 16664–16675. [[CrossRef](#)] [[PubMed](#)]
59. Jia, Y.; Zhang, Y.S.; Fu, J.G.; Yuan, L.X.; Li, Z.; Liu, C.; Zhao, D.; Wang, X.B. A novel magnetic biochar/MgFe-layered double hydroxides composite removing Pb²⁺ from aqueous solution: Isotherms, kinetics and thermodynamics. *Colloid Surf. A-Physicochem. Eng. Asp.* **2019**, *567*, 278–287. [[CrossRef](#)]
60. Faust, M.; Seipenbusch, M. Highly controlled structuring of Pt nanoparticles on TiO₂ and on ZrO₂ by a modified MOCVD process. *Surf. Coat. Technol.* **2014**, *259*, 577–584. [[CrossRef](#)]
61. Arthy, M.; Saravanakumar, M.P. Isotherm modeling, kinetic study and optimization of batch parameters for effective removal of Acid Blue 45 using tannery waste. *J. Mol. Liq.* **2013**, *187*, 189–200. [[CrossRef](#)]
62. Zama, E.F.; Zhu, Y.G.; Reid, B.J.; Sun, G.X. The role of biochar properties in influencing the sorption and desorption of Pb(II), Cd(II) and As(III) in aqueous solution. *J. Clean Prod.* **2017**, *148*, 127–136. [[CrossRef](#)]
63. Cantu, Y.; Remes, A.; Reyna, A.; Martinez, D.; Villarreal, J.; Ramos, H.; Trevino, S.; Tamez, C.; Martinez, A.; Eubanks, T.; et al. Thermodynamics, kinetics, and activation energy studies of the sorption of chromium(III) and chromium(VI) to a Mn₃O₄ nanomaterial. *Chem. Eng. J.* **2014**, *254*, 374–383. [[CrossRef](#)]
64. Wang, H.Y.; Gao, B.; Wang, S.S.; Fang, J.; Xue, Y.W.; Yang, K. Removal of Pb(II), Cu(II), and Cd(II) from aqueous solutions by biochar derived from KMnO₄ treated hickory wood. *Bioresour. Technol.* **2015**, *197*, 356–362. [[CrossRef](#)] [[PubMed](#)]
65. Lin, L.N.; Qiu, W.W.; Wang, D.; Huang, Q.; Song, Z.G.; Chau, H.W. Arsenic removal in aqueous solution by a novel Fe-Mn modified biochar composite: Characterization and mechanism. *Ecotoxicol. Environ. Saf.* **2017**, *144*, 514–521. [[CrossRef](#)] [[PubMed](#)]
66. Argun, M.E.; Dursun, S.; Ozdemir, C.; Karatas, M. Heavy metal adsorption by modified oak sawdust: Thermodynamics and kinetics. *J. Hazard. Mater.* **2007**, *141*, 77–85. [[CrossRef](#)] [[PubMed](#)]
67. Benzaoui, T.; Selatnia, A.; Djabali, D. Adsorption of copper (II) ions from aqueous solution using bottom ash of expired drugs incineration. *Adsorpt. Sci. Technol.* **2018**, *36*, 114–129. [[CrossRef](#)]
68. Mall, I.D.; Srivastava, V.C.; Agarwal, N.K. Removal of Orange-G and Methyl Violet dyes by adsorption onto bagasse fly ash—Kinetic study and equilibrium isotherm analyses. *Dyes. Pigment.* **2006**, *69*, 210–223. [[CrossRef](#)]
69. Jefferson, W.A.; Hu, C.Z.; Liu, H.J.; Qu, J.H. Reaction of aqueous Cu-Citrate with MnO₂ birnessite: Characterization of Mn dissolution, oxidation products and surface interactions. *Chemosphere* **2015**, *119*, 72–80. [[CrossRef](#)]
70. Zhang, Z.B.; Cao, X.H.; Liang, P.; Liu, Y.H. Adsorption of uranium from aqueous solution using biochar produced by hydrothermal carbonization. *J. Radioanal. Nucl. Chem.* **2013**, *295*, 1201–1208. [[CrossRef](#)]
71. Jin, J.; Li, S.W.; Peng, X.Q.; Liu, W.; Zhang, C.L.; Yang, Y.; Han, L.F.; Du, Z.W.; Sun, K.; Wang, X.K. HNO₃ modified biochars for uranium (VI) removal from aqueous solution. *Bioresour. Technol.* **2018**, *256*, 247–253. [[CrossRef](#)]
72. Tiwari, D.; Laldanwngliana, C.; Choi, C.H.; Lee, S.M. Manganese-modified natural sand in the remediation of aquatic environment contaminated with heavy metal toxic ions. *Chem. Eng. J.* **2011**, *171*, 958–966. [[CrossRef](#)]
73. Liu, Z.G.; Zhang, F.S. Removal of lead from water using biochars prepared from hydrothermal liquefaction of biomass. *J. Hazard. Mater.* **2009**, *167*, 933–939. [[CrossRef](#)] [[PubMed](#)]
74. Mukherjee, A.; Zimmerman, A.R.; Harris, W. Surface chemistry variations among a series of laboratory-produced biochars. *Geoderma* **2011**, *163*, 247–255. [[CrossRef](#)]
75. Dong, X.L.; Ma, L.N.Q.; Li, Y.C. Characteristics and mechanisms of hexavalent chromium removal by biochar from sugar beet tailing. *J. Hazard. Mater.* **2011**, *190*, 909–915. [[CrossRef](#)]
76. Yao, Q.; Yang, H.; Wang, B.; Xie, J. Effects of coexisting ions on adsorption of Pb²⁺ onto Bentonite/LS-g-AM-co-MAH. *Acta Mater. Compos. Sin.* **2016**, *33*, 2181–2186.
77. Cao, X.D.; Ma, L.N.; Gao, B.; Harris, W. Dairy-Manure Derived Biochar Effectively Sorbs Lead and Atrazine. *Environ. Sci. Technol.* **2009**, *43*, 3285–3291. [[CrossRef](#)]
78. Ding, Y.; Liu, Y.G.; Liu, S.B.; Li, Z.W.; Tan, X.F.; Huang, X.X.; Zeng, G.M.; Zhou, Y.Y.; Zheng, B.H.; Cai, X.X. Competitive removal of Cd(II) and Pb(II) by biochars produced from water hyacinths: Performance and mechanism. *RSC Adv.* **2016**, *6*, 5223–5232. [[CrossRef](#)]
79. Zhang, C.; Shan, B.Q.; Tang, W.Z.; Zhu, Y.Y. Comparison of cadmium and lead sorption by *Phyllostachys pubescens* biochar produced under a low-oxygen pyrolysis atmosphere. *Bioresour. Technol.* **2017**, *238*, 352–360. [[CrossRef](#)] [[PubMed](#)]

Disclaimer/Publisher’s Note: The statements, opinions and data contained in all publications are solely those of the individual author(s) and contributor(s) and not of MDPI and/or the editor(s). MDPI and/or the editor(s) disclaim responsibility for any injury to people or property resulting from any ideas, methods, instructions or products referred to in the content.